CP-violating Higgs boson ditau decays: Baryogenesis and Higgs factories

Shao-Feng Ge,[1,2,*] Gang Li,[3,†] Pedro Pasquini,[1,‡] and Michael J. Ramsey-Musolf[1,2,3,4,§]

[1]*Tsung-Dao Lee Institute and School of Physics and Astronomy, Shanghai Jiao Tong University, Shanghai 200240, China*

[2]*Key Laboratory for Particle Astrophysics and Cosmology (MOE) and Shanghai Key Laboratory for Particle Physics and Cosmology, Shanghai Jiao Tong University, Shanghai 200240, China*

[3]*Amherst Center for Fundamental Interactions, Department of Physics, University of Massachusetts, Amherst, Massachusetts 01003, USA*

[4]*Kellogg Radiation Laboratory, California Institute of Technology, Pasadena, California 91125, USA*

(Received 22 January 2021; accepted 26 March 2021; published 26 May 2021)

We demonstrate how probes of *CP*-violating observables in Higgs boson ditau decays at prospective future lepton colliders could provide a test of weak scale baryogenesis with significant discovery potential. Measurements at the Circular Electron Positron Collider, for example, could exclude a *CP* phase larger than 2.9° (5.6°) at 68% (95%) C.L. assuming the Standard Model value for magnitude of the tau lepton Yukawa coupling. Conversely, this sensitivity would allow for a 5σ discovery for 82% of the *CP* phase range $[0, 2\pi)$. The reaches of the Future Circular Collider for electrons and positrons (FCC-ee) and International Linear Collider are comparable. As a consequence, future lepton colliders could establish the presence of *CP* violation required by lepton flavored electroweak baryogenesis with at least 3σ sensitivity. Our results illustrate that Higgs factories are not just precision machines, but can also make $\mathcal{O}(1)$ measurement of the new physics beyond the Standard Model.

DOI: 10.1103/PhysRevD.103.095027

I. INTRODUCTION

The discovery of the Higgs boson at the Large Hadron Collider (LHC) [1,2] and subsequent measurements of its properties strongly favor the mechanism of electroweak symmetry breaking (EWSB) given by the Standard Model (SM) of particle physics. In particular, the SM predicts each Higgs boson-fermion Yukawa coupling to be purely real, with magnitude proportional to the fermion mass. However, LHC measurements have confirmed this prediction up to only $\mathcal{O}(10)\%$ precision [3–6], leaving considerable room for physics beyond the Standard Model (BSM) in Higgs boson-fermion interactions. Precision Higgs boson studies aim to explore these BSM possibilities. Proposed future lepton colliders, including the Circular Electron-Positron Collider (CEPC) [7], Future Circular Collider for electrons and positrons (FCC-ee) [8], and International Linear Collider (ILC) [9], are designed for this purpose.

The motivations for BSM Higgs interactions are well known, including solutions to the hierarchy problem, generation of neutrino mass, dark matter, and the cosmic baryon asymmetry (BAU). In what follows, we focus on the possibility that the observation of *CP*-violating effects in Higgs-tau lepton interactions at a future lepton collider could provide new insight into the BAU problem. As pointed out by Sakharov [10], a dynamical generation of the BAU requires three ingredients in the particle physics of the early Universe: (1) nonconserving baryon number, (2) out-of-equilibrium dynamics (assuming *CPT* conservation), and (3) *C* and *CP* violation. While the SM contains the first ingredient in the form of electroweak sphalerons, it fails to provide the needed out-of-equilibrium conditions and requisite *CP* violation. The presence of BSM physics in the dynamics of EWSB could remedy this situation—the electroweak baryogenesis (EWBG) scenario (for a recent review, see Ref. [11]). While flavor-diagonal *CP*-violating (CPV) interactions relevant to EWBG are strongly constrained by limits on permanent electric dipole moments (EDMs) of the electron, neutron, and neutral atoms [12,13], the landscape for flavor-nondiagonal CPV is less restricted. Here, we show that searches for CPV effects in the Higgs boson ditau decays at future lepton colliders could provide an interesting probe of "flavored EWBG" [14–18] in the lepton sector.

In addition to being theoretically well motivated in its own right, EWBG has the additional attraction of experimental testability. Modifications of the SM scalar

*gesf@sjtu.edu.cn
†ligang@umass.edu
‡ppasquini@sjtu.edu.cn
§mjrm@sjtu.edu.cn

sector necessary for the EWBG out-of-equilibrium conditions provide a rich array of signatures accessible at the LHC and prospective future colliders [19]. The signatures of CP violation could appear in either low- or high-energy experiments. Our present focus is on the possible modification of the τ Yukawa coupling by a nonzero CP phase Δ as defined in Eq. (2.1) below and the resulting impact on Higgs decay into a pair of τ leptons. In this context, it has been known for some time that the Δ phase can be measured at colliders [20–32]. An $\mathcal{O}(1)$ modulation in the relevant differential distribution allows very accurate determination of Δ. The measurements at the LHC can achieve a precision around 10° [33–39] at 95% confidence level (C.L.) by using the full data with 3 ab^{-1} of integrated luminosity. Future lepton colliders [40] can further improve the measurements with higher integrated luminosity, optimized energy for Higgs production, and cleaner environment. Indeed, it was shown that the projected sensitivity for the ILC can reach 4.3° [41] and 2.9° for the CEPC [42] at 1σ level. To our knowledge, a detailed study connecting this sensitivity to the BAU has yet to appear in the literature.

In this work we thus study the capability of the CEPC, FCC-ee, and ILC in probing Δ and the resulting prospects of testing lepton flavored EWBG scenario. The projected sensitivities at future lepton colliders are much better than the current LHC results [43]. In Sec. II, we first make detailed comparison of several observables (the neutrino azimuthal angle difference $\delta\phi_\nu$, the polarimeter $\delta\phi_r$, the acoplanarity ϕ^*, and the Θ variable) to show that the polarimeter [32,44] is not just the optimal choice for probing Δ but can also apply universally to both the $\tau \to \pi\nu$ and $\tau \to \rho\nu$ decay channels. Then we use a simplified smearing scheme to simulate the detector responses and use χ^2 minimization to find the physical solution of neutrino or tau momentum in Sec. III. Based on these, we find that the future lepton colliders can make 5σ discovery of a nonzero CP phase for 82% of the allowed range. With a combination of these channels, the 1σ sensitivities can reach 2.9°, 3.2°, and 3.8° at the CEPC, FCC-ee, and ILC, respectively. Our result is better than the previous study for the ILC [41] and the same as Ref. [42] for the CEPC. Notice that, although the leptonic decay mode of τ is also considered in addition to the two meson decay modes with more usable events, a matrix element based observable is adopted [42] instead of the polarimeter $\delta\phi_r$ as we do here, leading to accidentally the same result as ours. Finally, in Sec. IV, we follow Ref. [14] in analyzing the implications for a lepton flavored EWBG scenario with 3σ sensitivity for the presence of CP violation at the CEPC, FCC-ee, and ILC. We summarize our findings in Sec. V.

II. *CP* PHASE AND AZIMUTHAL ANGLE DISTRIBUTIONS

The SM predicts the Higgs couplings with other SM particles to be proportional to their masses, including the τ lepton, $-y_\tau/\sqrt{2}\bar{\tau}_L\tau_R h + \text{H.c.} = -m_\tau/v\bar{\tau}\tau h$, where h denotes the SM-like Higgs boson, $v = 246$ GeV is the vacuum expectation value (VEV), and m_τ is the tau lepton mass. Although y_τ is, in general, complex, its CP phase can be rotated away without leaving any physical consequences. However, this is not always true when going beyond the SM. Any deviation from the SM prediction, for either the τ Yukawa coupling magnitude or the CP phase, indicates new physics. We first study the CP phase measurement by explicitly comparing various definitions of differential distributions in this section and then the detector response behaviors in Sec. III. The influence of the Yukawa coupling magnitude deviation from the SM prediction will be discussed in later parts of this paper.

The τ Yukawa coupling can be generally parametrized as

$$\mathcal{L}_{h\tau\tau} = -\kappa_\tau \frac{m_\tau}{v}\bar{\tau}(\cos\Delta + i\gamma_5 \sin\Delta)\tau h, \tag{2.1}$$

with κ_τ being real and positive by definition, and $\Delta \in [0, 2\pi)$ in general. We will consider $\Delta \in [0, \pi]$ since the CP measurement is insensitive to the multiplication of κ_τ by -1 [33].

The SM prediction for τ Yukawa coupling can be recovered with $\kappa_\tau \to 1$ and $\Delta \to 0$. A nonzero value of the CP phase Δ indicates CP violation in the τ Yukawa coupling and can be connected to baryogenesis in the early Universe [14].

Because of the P- and T-violating nature of the second term in Eq. (2.1), the spin correlation among the two τ leptons from a Higgs decay is an especially interesting probe for constraining its value [23]. In practice, one cannot measure the τ lepton directly but must rely on its decay products. The two most promising channels are the τ decay into $\pi^\pm$ ($\tau^\pm \to \pi^\pm \nu_{\tau^\pm}$) and into $\rho^\pm$ ($\tau^\pm \to \rho^\pm \nu_{\tau^\pm} \to \pi^\pm \pi^0 \nu_{\tau^\pm}$), with $\nu_{\tau^-}(\nu_{\tau^+})$ being the neutrino (antineutrino) from the decay of $\tau^-(\tau^+)$. These two channels contribute 10.82% and 25.49% of a single τ decay branching fraction [45], respectively.

A. Observables

For each τ decay, one decay plane can be formed by its decay products. The generic azimuthal angle ϕ difference between the two decay planes is then a good observable for probing Δ, which can be expressed as

$$\frac{1}{\Gamma}\frac{d\Gamma}{d\delta\phi} = \frac{1}{2\pi}[1 + A\cos(2\Delta - \delta\phi)], \tag{2.2}$$

where the coefficient A depends on the choice of observable. Note that only for Δ differing from integer multiples of $\pi/2$, this distribution will contain a term odd in $\delta\phi$.

There exists a variety of observables that afford access to Δ, which appears as the azimuthal angle difference in two decay planes. Here we review several possibilities and discuss the rationale for our choice of one of them.

1. Neutrino azimuthal angle difference

For both τ leptons decaying into a single charged pion, $\tau^\pm \to \pi^\pm \nu_{\tau^\pm}$, the differential distribution of the neutrino momentum azimuthal angle difference [44] is

$$\frac{1}{\Gamma}\frac{d\Gamma(h\to\pi^+\pi^-\nu_\tau\bar{\nu}_\tau)}{d\delta\phi_\nu}=\frac{1}{2\pi}\left[1-\frac{\pi^2}{16}\cos(2\Delta-\delta\phi_\nu)\right], \quad (2.3)$$

where $\delta\phi_\nu \equiv \phi_\nu - \phi_{\bar{\nu}}$ and $\phi_\nu(\phi_{\bar{\nu}})$ are defined in the $\tau^-(\tau^+)$ rest frame. On the other hand, if both τ's decay to rho mesons, $\tau^\pm \to \rho^\pm(\to\pi^\pm+\pi^0)\nu_{\tau^\pm}$, the differential distribution of the neutrino azimuthal angle difference $\delta\phi_\nu$ becomes

$$\frac{1}{\Gamma}\frac{d\Gamma(h\to\rho^+\rho^-\nu_\tau\bar{\nu}_\tau)}{d\delta\phi_\nu}=\frac{1}{2\pi}\left[1-\frac{\pi^2}{16}\left(\frac{m_\tau^2-2m_\rho^2}{m_\tau^2+2m_\rho^2}\right)^2\cos(2\Delta-\delta\phi_\nu)\right], \quad (2.4)$$

with a non-negligible suppression factor $(m_\tau^2-2m_\rho^2)^2/(m_\tau^2+2m_\rho^2)^2 \sim 0.2$. As shown in Fig. 1, this significantly reduces the sensitivity to the *CP* phase Δ. The neutrino azimuthal angle difference $\delta\phi_\nu$ is a good observable for the $\tau\to\pi\nu_\tau$ decay, but not for the $\tau\to\rho\nu_\tau$ channel.

2. Polarimeter

The azimuthal angle difference is not necessarily the optimized choice and multiple definitions of azimuthal angle have been invented. In Refs. [32,41,44], the azimuthal angle difference between the *polarimeter* vectors $\mathbf{r}_\pm$ was studied. For the τ decays, the polarimeter vectors are defined as

$$\tau^\pm\to\pi^\pm\nu_{\tau^\pm}: \quad \mathbf{r}_\pm \equiv -\hat{\mathbf{p}}_{\nu_{\tau^\pm}}, \quad (2.5a)$$

$$\tau^\pm\to\rho^\pm(\to\pi^\pm\pi^0)\nu_{\tau^\pm}: \quad \mathbf{r}_\pm \equiv -\frac{1}{N_\pm}\left[\hat{\mathbf{p}}_{\nu_{\tau^\pm}}+\frac{2m_\tau}{m_\rho^2-4m_\pi^2}\frac{E_{\pi^\pm}-E_{\pi^0_\pm}}{E_{\pi^\pm}+E_{\pi^0_\pm}}(\mathbf{p}_{\pi^\pm}-\mathbf{p}_{\pi^0_\pm})\right], \quad (2.5b)$$

where $\mathbf{r}_\pm$ is calculated in the corresponding $\tau^\pm$ rest frame, $(E_{\pi^0_\pm}, \mathbf{p}_{\pi^0_\pm})$ is the π^0 momentum in the $\tau^\pm$ decay, and $N_\pm$ is a normalization factor to ensure $|\mathbf{r}_\pm|=1$. Then the differential distribution in Eq. (2.2) becomes

$$\frac{1}{\Gamma}\frac{d\Gamma}{d\delta\phi_r}=\frac{1}{2\pi}\left[1-\frac{\pi^2}{16}\cos(2\Delta-\delta\phi_r)\right], \quad (2.6)$$

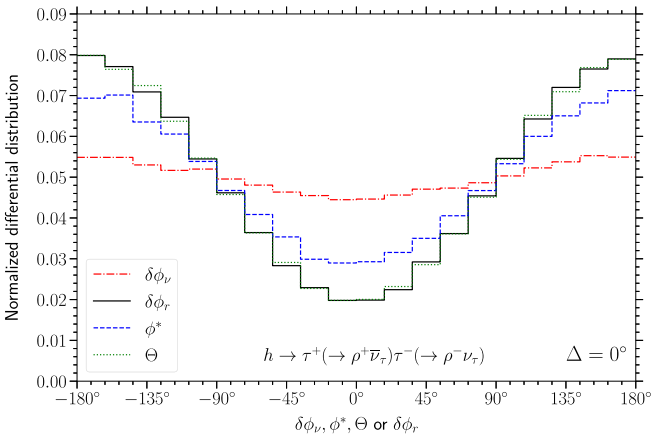

FIG. 1. The differential distributions of $h\to\tau^+(\to\rho^+\bar{\nu}_\tau)\times\tau^-(\to\rho^-\nu_\tau)$ for neutrino momentum $\delta\phi_\nu$ (red), polarimeter $\delta\phi_r$ (black), acoplanarity ϕ^* (blue), and the Θ variable (green) at the truth level for $\Delta=0°$.

for both decay channels including the mixed mode, $h\to\rho^\pm\pi^\mp\nu_\tau\bar{\nu}_\tau$. From the neutrino azimuthal angle difference $\delta\phi_\nu$ in Eq. (2.4) to the one of the polarimeter in Eq. (2.6), the amplitude gets amplified by a factor of 5, which is a significant improvement.

The azimuthal angle difference $\delta\phi_r \equiv \phi_{\mathbf{r}_+} - \phi_{\mathbf{r}_-}$ is defined with respect to the z direction, $\mathbf{z}\equiv\hat{\mathbf{p}}_{\tau^-}$. In the Higgs rest frame,

$$\tan\delta\phi_r = \frac{\hat{\mathbf{p}}_{\tau^-}\cdot(\mathbf{r}_+\times\mathbf{r}_-)}{\mathbf{r}_-\cdot\mathbf{r}_+-(\mathbf{r}_+\cdot\hat{\mathbf{p}}_{\tau^-})(\mathbf{r}_-\cdot\hat{\mathbf{p}}_{\tau^-})}. \quad (2.7)$$

For the $\tau^\pm\to\pi^\pm\nu_{\tau^\pm}$ decay channel, the polarimeter is along the neutrino momentum direction, namely, $\mathbf{r}_\pm=-\hat{\mathbf{p}}_{\nu_{\tau^\pm}}$ as shown in Eq. (2.5a). When ditau decay into pions, it is the azimuthal angle difference ϕ_ν. In contrast, the polarimeter for the $\tau^\pm\to\rho^\pm\nu_{\tau^\pm}$ decay channel does not coincide with any momentum of the final-state particles. For illustration, the distribution of $\delta\phi_r$ for $h\to\tau^+(\to\rho^+\bar{\nu}_\tau)\tau^-(\to\rho^-\nu_\tau)$ is shown in Fig. 1.

The four-vector $r_\pm=(0,\mathbf{r}_\pm)$ serves as the effective spin of the corresponding $\tau^\pm$ leptons. This becomes evident in the total matrix element of the Higgs decay chain,

$$|\mathcal{M}^{\text{total}}|^2 \propto \text{Tr}[(\not{p}_{\tau^-}+m_\tau)(1+\gamma_5\not{r}_-)\times\mathcal{O}(\not{p}_{\tau^+}-m_\tau)(1-\gamma_5\not{r}_+)\bar{\mathcal{O}}], \quad (2.8)$$

with $\mathcal{O} \equiv \cos\Delta + i\gamma_5 \sin\Delta$, $\bar{\mathcal{O}} \equiv \gamma^0 \mathcal{O}^\dagger \gamma^0$, and $p_{\tau^\pm} \equiv (E_{\tau^\pm}, \mathbf{p}_{\tau^\pm})$ being the momentum of $\tau^\pm$. If the Higgs boson decays to polarized τ leptons, it should be the τ spin vector $s_\pm = (|\mathbf{p}_{\tau^\pm}|/m_\tau, E_{\tau^\pm}/m_\tau \hat{\mathbf{p}}_{\tau^\pm})$ that appears in place of the polarimeter $r_\pm$. But since the Higgs decay chain also contains contribution from the τ decays, $s_\pm$ is replaced by $r_\pm$ to take the extra effects into consideration.

3. Acoplanarity

This observable was introduced in Refs. [22,23] for the $\tau \to \rho\nu_\tau$ decay mode. In the rest frame of the $\rho^+\rho^-$ system, the ρ momenta are back to back. The decay products of $\rho^\pm$ form two decay planes and the angle difference between them is defined as *acoplanarity* ϕ^*,

$$\tan\phi^* \equiv \frac{\hat{\mathbf{p}}_{\rho^-} \cdot [(\mathbf{p}_{\pi^+} \times \mathbf{p}_{\pi^0_+}) \times (\mathbf{p}_{\pi^-} \times \mathbf{p}_{\pi^0_-})]}{(\mathbf{p}_{\pi^+} \times \mathbf{p}_{\pi^0_+}) \cdot (\mathbf{p}_{\pi^-} \times \mathbf{p}_{\pi^0_-})}. \tag{2.9}$$

This interesting variable requires only the knowledge of the directly observable momenta of $\pi^\pm$ and π^0. However, the oscillation amplitude of the distribution is suppressed by around 30% in comparison with the polarimeter as shown in Fig. 1.

4. The Θ variable

For $\tau \to \rho\nu_\tau$ decay, a fourth observable similar to the usual acoplanarity angle, can be defined as

$$\tan\Theta \equiv \frac{\hat{\mathbf{p}}_{\tau^+} \cdot (\mathbf{E}_+ \times \mathbf{E}_-)}{\mathbf{E}_- \cdot \mathbf{E}_+ - (\mathbf{E}_+ \cdot \hat{\mathbf{p}}_{\tau^+})(\mathbf{E}_- \cdot \hat{\mathbf{p}}_{\tau^+})}, \tag{2.10}$$

with $\mathbf{E}_\pm$ taking analogy to the electromagnetic fields. In the $\tau^\pm$ rest frames, the $\mathbf{E}_\pm$ vector can be expressed as [33]

$$\mathbf{E}_\pm \equiv \frac{m_\rho^2 - 4m_\pi^2}{2m_\tau}\left[\frac{m_\tau^2 - m_\rho^2}{m_\tau^2 + m_\rho^2}\hat{\mathbf{p}}_{\nu_{\tau^\pm}} + \frac{2m_\tau}{m_\rho^2 - 4m_\pi^2}\frac{(E_{\pi^\pm} - E_{\pi^0})}{(E_{\pi^\pm} + E_{\pi^0})}(\mathbf{p}_{\pi^\pm} - \mathbf{p}_{\pi^0_\pm})\right]. \tag{2.11}$$

Note that Eq. (2.10) is slightly more general than the one presented in Ref. [33], where they take the approximation $(\mathbf{E}_\pm \cdot \hat{\mathbf{p}}_{\tau^\pm}) \approx 0$. It is very interesting to see that Eq. (2.10) has very similar form as Eq. (2.7) with the only difference of a proportional factor $(m_\rho^2 - 4m_\pi^2)/2m_\tau$. Because of these similarities, the Θ variable has roughly the same sensitivity as the polarimeter, see Fig. 1.

The comparison in Fig. 1 shows that the polarimeter $\delta\phi_r$ and the Θ variable are the optimal ones. However, the Θ variable needs both momenta of $\pi^\pm$ and π^0, limiting its scope to only the $\tau \to \rho\nu_\tau$ decay mode. In contrast, the polarimeter method applies for both channels by matching $\mathbf{r}_\pm$ with different combinations of final-state particle momenta as shown in Eq. (2.5). So we adopt the polarimeter scheme in the following part of this paper.

III. MEASUREMENTS AT FUTURE LEPTON COLLIDERS

Future lepton colliders [46] are designed to produce millions of Higgs events. The three prominent candidate colliders are the CEPC [7], FCC-ee [8], and ILC [47]. The CEPC experiment [7] is expected to have around 1.1×10^6 Higgs events. This comes from an integrated luminosity of 5.6 ab^{-1} with two interaction points and seven years of running at $\sqrt{s} = 240$ GeV. The FCC-ee has a higher luminosity and four interaction points, but runs in the Higgs factory mode for only three years, resulting in a 5 ab^{-1} of integrated luminosity or equivalently 1.0×10^6 Higgs events [8]. The ILC, on the other hand, has a significantly lower integrated luminosity at 2 ab^{-1}, but is able to produce polarized electrons and positrons, which increases the cross section significantly, effectively raising its number of Higgs production to 0.64×10^6 [9]. The configuration of these three experiments and the expected numbers of Higgs events at the benchmark luminosities have been summarized in Table I for comparison.

In this section, we study the detector responses, including the smearing effects, selection cuts, and momentum reconstruction ambiguities. With around 650–1100 events, the uncertainty at the level of 14%–18% is much smaller than the expected 60% modulation in the CP measurement. This allows a 5σ discovery potential for approximately 80% of the allowed range in $[0, 2\pi)$ of the CP phase Δ and a determination of Δ with the accuracy of 2.9°–3.8°.

A. Simulation and detector responses

At lepton colliders, the Higgs boson is mainly produced in the so-called Higgsstrahlung process, $e^+e^- \to Zh$, with an associated Z boson. This channel allows a model-independent measurement of the Higgs properties thanks to the recoil mass reconstruction method [48]. The Higgs event is first selected by reconstructing the Z boson without assuming any Higgs coupling with the SM particles. The Higgs boson momentum can be either derived from the Z boson momentum using energy-momentum conservation or reconstructed from the Higgs decay products. Since there are always two neutrinos in the final state of $h \to \tau\tau$

TABLE I. Configurations (integrated luminosity, energy $\sqrt{s}$, and Higgs production rate) at the future lepton colliders CEPC, FCC-ee, and ILC.

	Integrated luminosity (ab^{-1})	$\sqrt{s}$ (GeV)	No. Higgs bosons ($\times 10^6$)
CEPC [7]	5.6	240	1.1
FCC-ee [8]	5	240	1.0
ILC [9]	2	250	0.64

events, the Z boson momentum is needed to reconstruct the Higgs momentum as the initial condition of the Higgs decay kinematics to fully recover the two neutrino momenta.

We use MadGraph [49] and TauDecay [50] packages to simulate the spin correlation in the Higgs decay chains. For a realistic simulation, both detector response and statistical fluctuations have to be taken into consideration. In order to perform fast detector simulation, we construct a simplified smearing algorithm that is validated by comparing with DELPHES [51] output.

Using the recoil mass method, the smearing should, in principle, be applied to the Z momentum. Nevertheless, since the Higgs and Z bosons are back to back in the center of mass frame, we can directly smear the Higgs momentum. Defining the z axis along the Higgs momentum, only its P_z component is affected by the Z boson decay modes, while the other two, P_x and P_y, have independent smearing behaviors. To select the Higgsstrahlung events, those with the reconstructed Z-invariant mass outside the range $80 < \sqrt{p_Z^2} < 100$ GeV are discarded. The momentum uncertainties of Higgs smearing have been summarized in Table II.

The pion momentum smearing is performed by randomly sampling the azimuthal angle ϕ and the pseudorapidity η according to Gaussian distribution [51,52]. In addition, the transverse momentum $|\mathbf{p}_T|$ is sampled with a log-normal-like distribution from Ref. [51],

$$|\mathbf{p}_T^{\mathrm{rec}}| = \exp\left(\log|\mathbf{p}_T| - \frac{\epsilon}{2}\sqrt{1+\frac{\sigma^2}{|\mathbf{p}_T|^2}}\right), \qquad (3.1)$$

with ϵ being a random number following a Gaussian distribution centered in 0 with error 1 and N a normalization factor. For τ decay into $\rho^{\pm}$, the reconstructed ρ-invariant mass is required to be within the range of $0.3 < \sqrt{p_\rho^2} < 1.2$ GeV. The uncertainties of $(\phi, \eta, |\mathbf{p}_T|)$ for pions are summarized in Table III.

Although our simplified smearing algorithm is admittedly less sophisticated, our results are broadly compatible with those commonly adopted in the literature. A complete analysis in momentum reconstruction and detailed cuts was performed in Refs. [42,51]. For validation, we compare our smearing algorithm to the DELPHES simulation with the configurations cards `delphes_card_CircularEE.tcl` [53] for the CEPC and FCC-ee [55] and `delphes_card_ILD.tcl` [54] for the ILC. Figure 2 shows the smeared distributions of the pion kinematic variables simulated with DELPHES (black) vs our simplified smearing (blue). We can see that the results of these two simulations agree with each other quite well. In this work, we take the simplified smearing algorithm for a fast simulation.

TABLE II. Uncertainties of the Higgs boson [42].

Higgs smearing	
Observables	Uncertainty (GeV)
$P_{x,y}$	1.82
$P_z\ (Z \to jj)$	2.3
$P_z\ (Z \to l\bar{l})$	0.57

TABLE III. Pion momentum smearing parameters to be consistent with the DELPHES configurations `delphes_card_CircularEE.tcl` [53] for the CEPC/FCC-ee and `delphes_card_ILD.tcl` [54] for the ILC.

Pion smearing	
Observables	Uncertainty
ϕ	$0.0002\lvert\eta\rvert + 0.000022$
η	$0.000016\lvert\eta\rvert + 0.00000022$
$\lvert\mathbf{p}_T\rvert$	$0.036\lvert\mathbf{p}_T\rvert$

To obtain the total number of expected events, one needs to consider several branching ratios. First, the Z boson can only be reconstructed if it decays into either leptons or jets with 80% of branching ratio in total [45]. Also, since the decay branching ratio of Higgs decaying into two τ leptons is 6.64% [45], only around 5.3% of the actual Higgs events associated with Z production are available for the CP measurement. Further suppression comes from the branching fraction of the decay of τ into π or ρ. We arrive at 7704 events at the CEPC, 7003 events at the FCC-ee, and 4482 events at the ILC. Taking into account the identification of τ jets and tagging of the Higgs boson and other selection cuts [41], we obtain an overall efficiency $\epsilon = 0.145$, 0.144, and 0.142 for (π,π), (π,ρ), and (ρ,ρ) decay modes, respectively.

The expected event numbers before and after applying the selection efficiencies are shown in Tables IV and V for comparison. In total, roughly 1105, 1004, and 643 events of the $h \to \tau^+\tau^-, \tau^\pm \to \pi^\pm/\rho^\pm\nu_{\tau^\pm}$ decay chains can be reconstructed at the CEPC, FCC-ee, and ILC, respectively.

B. Ambiguities in momentum reconstruction

Experimentally, in order to reconstruct the τ momentum, it is unavoidable to first obtain the neutrino momentum, which is not directly detectable. With two neutrinos in the final state, we need to constrain 2 four-vector momenta. Since the Higgs momentum can be fully reconstructed from the Z boson counterpart, only one neutrino momentum is independent due to energy-momentum conservation. The 4 degrees of freedom can be constrained by the on-shell conditions of the two neutrinos and the two τ leptons.

Unfortunately, the solutions have a twofold ambiguity. Since on-shell conditions are in quadratic forms, one sign cannot be uniquely fixed. For completeness, we summarize the solution here in terms of the τ^- momentum defined in the Higgs rest frame,

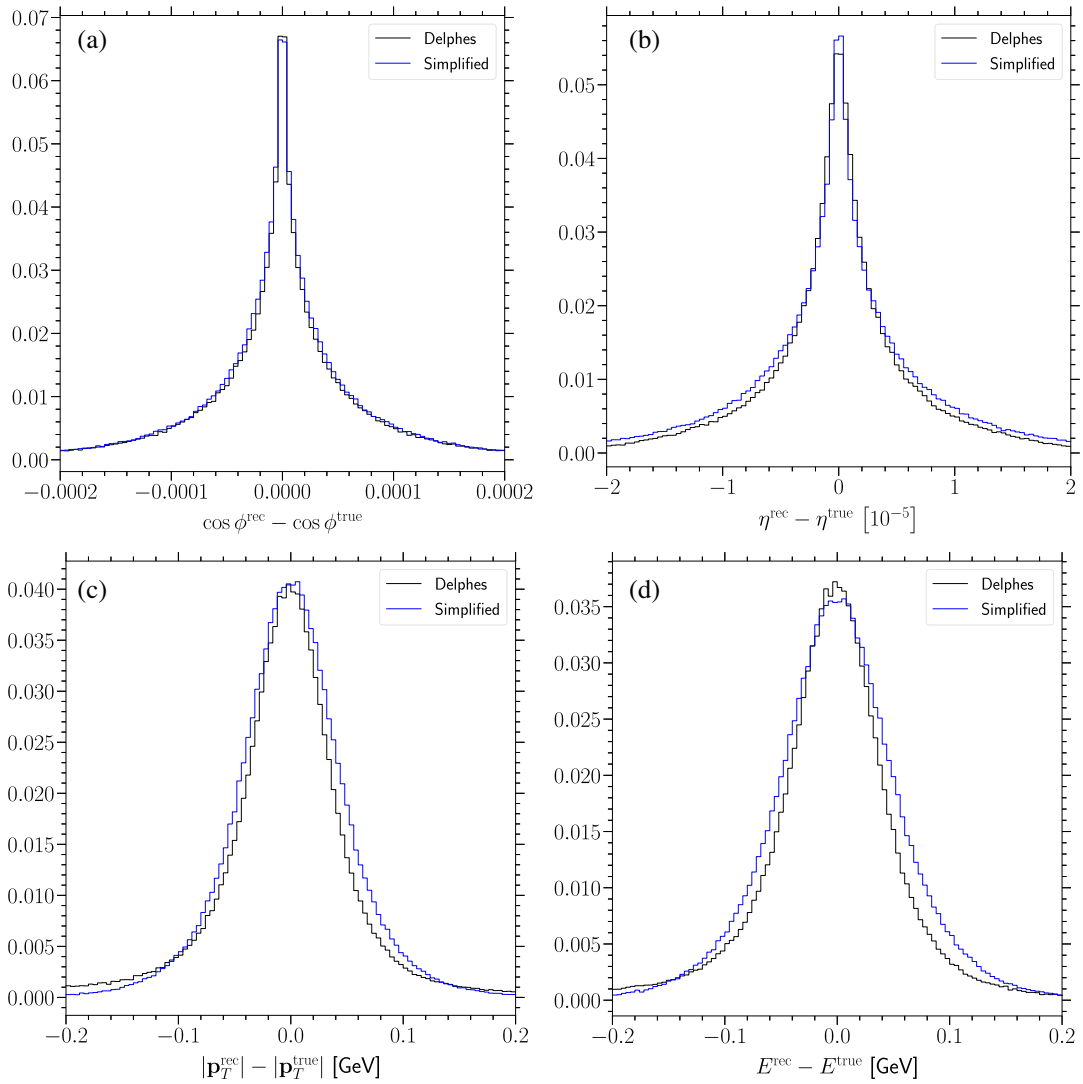

FIG. 2. The pion smearing effects simulated by DELPHES (black) and our simplified algorithm (blue). Panel (a) (b) (c) (d) correspond to the comparison of the cos ϕ, η, $|p_T|$, and E of pions obtained using Delphes and our simplified smearing. Notice that in (b), the numbers in the horizontal axis are multiplied by a factor $\times 10^5$ for better visualization.

$$\mathbf{p}_{\tau_-} = \sqrt{p_h^2 - 4m_\tau^2}[\sin\theta_\tau(\cos\phi_\tau\hat{\mathbf{n}}_1 + \sin\phi_\tau\hat{\mathbf{n}}_2) \pm \cos\theta_\tau\hat{\mathbf{n}}_3]. \tag{3.2}$$

The unit base vectors $\hat{\mathbf{n}}_i$ are constructed in terms of the primary decay mesons, $X_\pm \equiv \pi^\pm, \rho^\pm$,

TABLE IV. Branching fractions associated with the entire reaction. The values were obtained from [45].

Decay modes	Branching ratio (%)
$Z \to$ vis.	8
$h \to \tau^+\tau^-$	6.64
$\tau \to \pi\nu_\tau$	10.82
$\tau \to \rho\nu_\tau$	25.49

TABLE V. Expected event numbers at the CEPC [7] with the integrated luminosity $\mathcal{L} = 5.6$ ab^{-1}, FCC-ee [8] with $\mathcal{L} = 5$ ab^{-1}, and ILC [47] with $\mathcal{L} = 2$ ab^{-1}. The expected numbers of events before and after selection cuts are shown in the columns "before" and "after," respectively, with the overall cut efficiencies taken from Ref. [41].

	Number of Higgs decay events					
	CEPC		FCC-ee		ILC	
τ decay products	Before	After	Before	After	Before	After
(π,π)	684	99	622	90	398	58
(π,ρ)	3223	465	2930	423	1875	271
(ρ,ρ)	3797	541	3451	491	2209	314

$$\hat{\mathbf{n}}_1 = \hat{\mathbf{p}}_{X_+}, \qquad \hat{\mathbf{n}}_2 = \frac{\hat{\mathbf{p}}_{X_-} - (\hat{\mathbf{p}}_{X_+}\cdot\hat{\mathbf{p}}_{X_-})\hat{\mathbf{p}}_{X_+}}{\sqrt{1-(\hat{\mathbf{p}}_{X_+}\cdot\hat{\mathbf{p}}_{X_-})^2}},$$
$$\hat{\mathbf{n}}_3 = \frac{\hat{\mathbf{p}}_{X_+}\times\hat{\mathbf{p}}_{X_-}}{\sqrt{1-(\hat{\mathbf{p}}_{X_+}\cdot\hat{\mathbf{p}}_{X_-})^2}}. \tag{3.3}$$

The first base vector $\hat{\mathbf{n}}_1$ is along the momentum of π^+ or ρ^+, while the third one $\hat{\mathbf{n}}_3$ is perpendicular to the momentum of both primary mesons. Finally, $\hat{\mathbf{n}}_2$ is simply the one perpendicular to both $\hat{\mathbf{n}}_1$ and $\hat{\mathbf{n}}_3$. The polar angles of the τ momentum can be reconstructed as

$$\sin\theta_\tau\cos\phi_\tau = \frac{m_\tau^2 + m_X^2 - m_h E_{X_+}}{|\mathbf{p}_{X_+}|\sqrt{m_h^2-4m_\tau^2}}, \tag{3.4a}$$

$$\sin\theta_\tau\sin\phi_\tau = \frac{m_h E_{X_-} - m_\tau^2 - m_{X_-}^2}{|\mathbf{p}_{X_-}||s_{X_-X_+}|\sqrt{m_h^2-4m_\tau^2}} + \frac{m_h E_{X_+} - m_\tau^2 - m_{X_+}^2}{|\mathbf{p}_{X_+}||s_{X_-X_+}|\sqrt{m_h^2-4m_\tau^2}} c_{X_-X_+}, \tag{3.4b}$$

where $(s_{X_-X_+}, c_{X_-X_+}) \equiv (\sin\theta_{X_-X_+}, \cos\theta_{X_-X_+})$ and $\theta_{X_-X_+}$ is the angle between the momentum of X_+ and X_-.

However, in Eq. (3.2) the $\pm$ sign in front of $\hat{\mathbf{n}}_3$ reflects the fact that both solutions obey all the constraints from energy-momentum conservation and the correct solution cannot be unambiguously obtained. This sign ambiguity can significantly decrease the *CP* sensitivity, especially for the neutrino azimuthal angle distribution. Using momentum conservation, the result in Eq. (2.7) for $\tan\delta\phi_\nu$ can be written in the same form by substituting $\mathbf{p}_\nu$ by $\mathbf{p}_{X^\pm}$, hence, $\tan\delta\phi_\nu \propto \hat{\mathbf{p}}_{\tau^-}\cdot(\mathbf{p}_{X^+}\times\mathbf{p}_{X^-}) = \pm\cos\theta_\tau/\sqrt{1-(\hat{\mathbf{p}}_{X_+}\cdot\hat{\mathbf{p}}_{X_-})^2}$. In other words, $\delta\phi_\nu$ can have both positive and negative solutions with the same magnitude. This would not be a big problem for the symmetric distribution of $\delta\phi_\nu$ around its origin, such as those curves in Fig. 1 with $\Delta = 0°$, but it causes significant issues for other Δ values and effectively flattens the curve for $\Delta = \pm 45°$.

This ambiguity can be solved by measuring other decay information. An especially useful quantity is the impact parameter [56,57], the minimum distance of charged meson trajectory to the τ leptons production point. The impact parameter measurement essentially removes the twofold ambiguity for the τ Yukawa *CP* measurement at future lepton colliders [24,52]. A more recent study with spatial resolution of 5 μm can be found in Refs. [41,42].

Another ambiguity comes from the detector resolutions. The τ momentum is reconstructed from the smeared Higgs and meson momentum. This reconstruction is realized with energy and momentum conservation, assuming narrow width approximation for the τ momentum, $p_{\tau^\pm}^2 = m_\tau^2$. Both smearing and finite width could lead to nonphysical solutions in Eq. (3.4), for example, $\sin\theta_\tau\sin\phi_\tau > 1$. For those events, we follow a similar procedure introduced in Ref. [42]. We try to find the solution for the (anti)neutrino momenta optimally consistent with all the information we have on each event (including four-momentum conservation) by minimizing the function

$$\chi^2_{\rm rec} = \sum_{i=0}^{3}\left(\frac{(p^{\rm rec}_{\tau^+})_i + (p^{\rm rec}_{\tau^-})_i - (p^{\rm rec}_h)_i}{\sigma_h}\right)^2 + \left(\frac{(p^{\rm rec}_{\tau^+})^2 - m_\tau^2}{\sigma_\tau}\right)^2 + \left(\frac{(p^{\rm rec}_{\tau^-})^2 - m_\tau^2}{\sigma_\tau}\right)^2, \tag{3.5}$$

where $i = 0, \ldots, 3$ runs over the four-momentum components of each particle momentum. We adopt the uncertainties as $\sigma_h = 4.0$ and $\sigma_\tau = 0.2$ GeV [42]. The $\chi^2_{\rm rec}$ function is minimized over the six kinematic parameters of the unmeasured neutrino momentum: the pseudorapidity, azimuthal angle, and absolute value of the momentum for both neutrino and antineutrino. Then the τ momentum is then obtained with energy-momentum conservation, $p^{\rm rec}_{\tau^\pm} = p_{\nu^\pm} + p^{\rm rec}_{X^\pm}$. The best fit at the minimum of $\chi^2_{\rm rec}$ approximates the physical solution. We keep the event if the minimum solution is consistent with the mass cuts. Otherwise, the event is discarded.

The final result of the differential distribution for the $h \to \tau^+(\to\rho^+\bar{\nu}_\tau)\tau^-(\to\rho^-\nu_\tau)$ process is plotted in Fig. 3. The left panel shows the differential distributions for $\Delta = 0°$ (red), $\Delta = 45°$ (blue), and $\Delta = 90°$ (green), respectively. Being divided into 20 bins [33,41], there are 25–35 events in each bin on average. The corresponding statistical uncertainty at the level of 17%–20% is much smaller than the oscillation amplitude, $\pi^2/16 \approx 62\%$. The event rate at the CEPC is large enough to constrain the modulation pattern as elaborated in Sec. III C. The right panel shows the spectrum at the three future candidate lepton colliders, CEPC (red), FCC-ee (blue), and ILC (green), respectively, for comparison. While CEPC and FCC-ee have comparable spectrum, ILC has much lower event rate and hence larger fluctuations.

It is interesting to see that, for $\Delta = 90°$, the differential distribution of $\delta\phi_r$ has only $\cos\delta\phi_r$ but no $\sin\delta\phi_r$ in Eq. (2.6). In other words, the observable that we measure has only *CP*-conserving contribution that does not change under *CP* transformation. However, the distributions in the left panel of Fig. 3 show that the difference between $\Delta = 0°$ and $\Delta = 90°$ is maximal. This is because $\cos 2\Delta = \pm 1$ take the two extreme values with opposite signs.

C. Discovery potential and sensitivity of the *CP* phase

To evaluate the *CP* measurement sensitivities, we adopt a χ^2 function defined according to the Poisson distribution,

$$\chi^2 \equiv \sum_i 2(N_i^{\rm test} - N_i^{\rm true}) + 2N_i^{\rm true}\log(N_i^{\rm true}/N_i^{\rm test}), \tag{3.6}$$

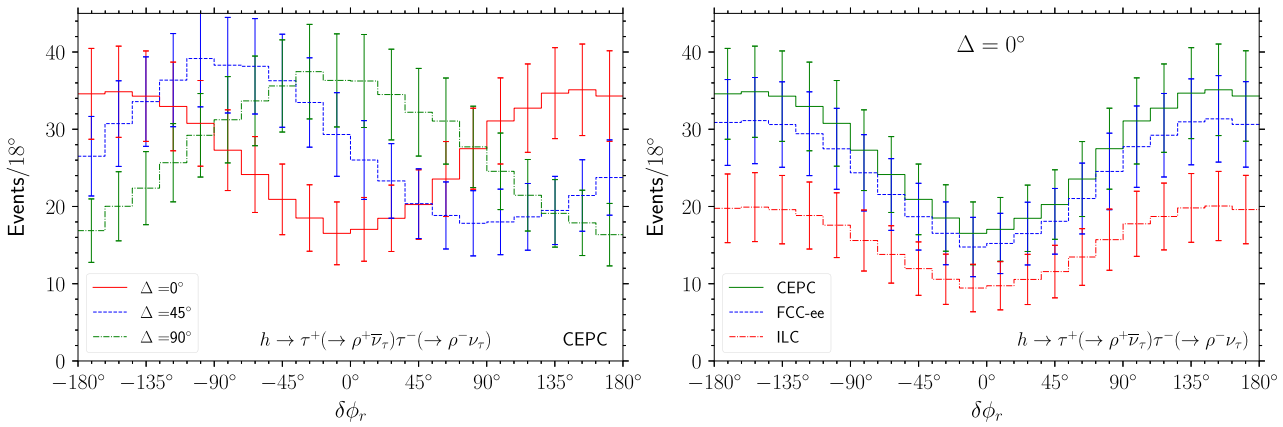

FIG. 3. Smeared differential distributions of $\delta\phi_r$ in the decay mode $h \to \tau^+(\to \rho^+\bar{\nu}_\tau)\tau^-(\to \rho^-\nu_\tau)$. Left: the distribution for CP phases $\Delta = 0°$ (red), $\Delta = 45°$ (blue), $\Delta = 90°$ (green) at the CEPC. Right: a comparison of the distributions at the CEPC (red), FCC-ee (blue), and ILC (green) for $\Delta = 0°$. In both panels, the error bars indicate the statistical uncertainties.

where $i = 1, \ldots, 20$ runs over all the 20 bins of the $\delta\phi_r$ differential distribution. Since we are studying the projected sensitivity at future lepton colliders, there is no real data available yet. Instead, we simulate the measurement with some assumed true values of the CP phase Δ to produce a set of pseudodata N_i^{true} and then fit these pseudodata with some test values N_i^{test}. The event numbers N_i^{true} and N_i^{test} are functions of the true value Δ^{true} and Δ^{test}, respectively.

The discovery ability of a nonzero CP phase can be parametrized as the smaller one of the two χ^2 values between the given Δ^{true} and the CP conserving cases $\Delta^{\text{test}} = 0°$ or $\Delta^{\text{test}} = 180°$,

$$\chi^2_{\text{CPV}}(\Delta^{\text{true}}) \equiv \min[\chi^2(\Delta^{\text{true}}, \Delta^{\text{test}} = 0°), \chi^2(\Delta^{\text{true}}, \Delta^{\text{test}} = 180°)]. \quad (3.7)$$

Figure 4 shows the $\sqrt{\chi^2_{\text{CPV}}}$ distribution as a function of Δ assuming $\kappa_\tau = 1$. The sensitivities for the ditau decay into (ρ,ρ), $(\rho,\rho)+(\pi,\rho)$, and the full combination $(\rho,\rho)+(\pi,\rho)+(\pi,\pi)$ are depicted in light green, green, and dark green regions, respectively. For different decay channels, the differential distributions have the same amplitude $\pi^2/16$ as indicated in Eq. (2.6). The gray area corresponds to the currently allowed region of Δ at 95% C.L. from the CP measurement in $h \to \tau^+\tau^-$ at the LHC [43]. The main difference in the sensitivities of each channel is due to the event rates: the branching ratio of the $\tau \to \pi\nu_\tau$ is only 10.8%, in comparison with the 25% for the $\tau \to \rho\nu_\tau$ channel. As indicated by the black dashed lines, 95% of the values of Δ can be tested above 95% C.L. and 82% of the parameter space can be tested at even more than 5σ. The sensitivity peaks at $\Delta = \pm 90°$ where Eq. (2.6) takes the most different value from that of $\Delta = 0°$ or 180° with more

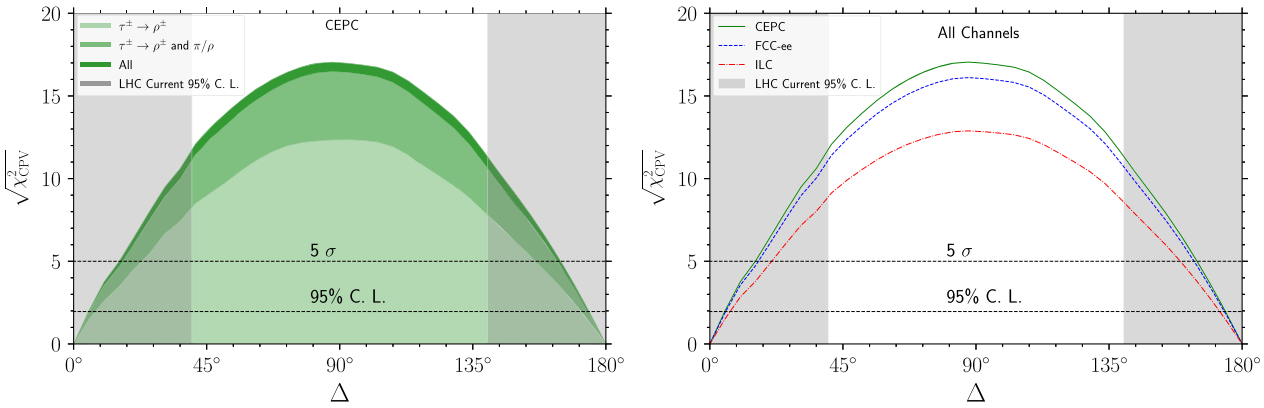

FIG. 4. Left: the CP phase discovery potential at the CEPC for $\kappa_\tau = 1$. The green shaded regions represent the results from various decay modes: only (ρ,ρ) (light green), $(\rho,\rho)+(\pi,\rho)$ (green), and the fully combined one $(\rho,\rho)+(\pi,\rho)+(\pi,\pi)$ (dark green), with the boundaries describing the $\sqrt{\chi^2_{\text{CPV}}}$ values according to Eq. (3.7) given Δ^{true}. The black dashed lines with $\sqrt{\chi^2_{\text{CPV}}} = 1.96, 5$ mark the sensitivities at 95% C.L. and 5σ, respectively. Right: sensitivity of all the channels at the CEPC (green), FCC-ee (blue), and ILC (red). In both panels, the region outside of the gray bands are excluded at 95% C.L. by the current CP measurement at the LHC [43].

TABLE VI. Our results on the *CP* phase precision at the CEPC, FCC-ee, and ILC for m parameter(s) and given integrated luminosity. This results were obtained by including the (ρ,ρ), (ρ,π), and (π,π) channels in the analysis.

	68% C.L. for $m=1$ (°)	95% C.L. for $m=1$ (°)	95% C.L. for $m=2$ (°)	Luminosity (ab^{-1})
CEPC	2.9	5.6	7.0	5.6
FCC-ee	3.2	6.3	7.8	5
ILC	3.8	7.4	9.3	2

than 10σ significance. In the right panel, we also show the comparison of the sensitivities at the CEPC (green), FCC-ee (blue), and ILC (red). As expected, the CEPC has the highest sensitivity due to the higher number of events.

For completeness, Table VI summarizes the expected precision of the Δ measurement at future lepton colliders at 68% and 95% C.L. for $m=1$ parameter (Δ) or $m=2$ parameters (Δ and κ_τ). In previous studies for the ILC, the 1σ sensitivity is 4.4° with 1 ab^{-1} in only the $\tau\to\rho\nu_\tau$ decay channel [33] or 4.3° with 2 ab^{-1} in both τ decay channels [41]. For the CEPC, our result is the same as the 2.9° in Ref. [42]. Notice that, in addition to $\tau\to\rho\nu,\pi\nu$, the leptonic decay channel $\tau\to\ell\nu\bar{\nu}$ is also considered in Ref. [42] with the matrix element based observable $\phi_{\rm ME}$ that is different from our polarimeter $\delta\phi_r$. In Ref. [31], both the leptonic channels and the $\tau^\pm\to a_1^\pm(\to 3\pi)\nu_{\tau^\pm}$ decay modes are considered in addition to those analyzed here. Their combined result reaches 2.8° with more decay channels and event numbers. To make a direct comparison, we take only the (ρ,ρ) decay mode whose resolution was explicitly given in Ref. [31], with the same resolution around 7° as ours. Notice that in Ref. [31], their number of events in the (ρ,ρ) decay mode is 40% larger than ours due to different selection cuts. It indicates that we achieve the same sensitivities with less signal events in the (ρ,ρ) decay mode by using the polarimeter $\delta\phi_r$, in contrast with the acoplanarity parameter ϕ^* used in Ref. [31]. We can clearly see from Table VI that the future lepton colliders can differentiate the CPV scenario from the *CP*-conserving one very well.

IV. PROSPECTS OF CONSTRAINING NEW PHYSICS

As the aforementioned analysis shows, there remains significant potential for discovering *CP* violation in the $h\to\tau^+\tau^-$ decay at prospective future lepton colliders. We now draw the connection with the lepton flavored EWBG scenario, following the treatment given in Ref. [14] for concrete illustration (see Refs. [15–18]).This discussion exemplifies that future lepton colliders are not only precision machines, but can also make an $\mathcal{O}(1)$ measurement of BSM physics effects.

A. Two Higgs doublet model

The setup in Ref. [14] relies on the type III two Higgs doublet model (THDM) [58,59], wherein the two scalar doublet fields before EWSB are denoted as $\Phi_{1,2}$. Both neutral scalars inside $\Phi_{1,2}$ acquire nonzero VEVs, v_1 and v_2, respectively, with $v\equiv\sqrt{v_1^2+v_2^2}=246$ GeV. The neutral components can mix with each other to form three neutral massive scalar fields after one neutral Goldstone boson is eaten by the Z boson. We assume a *CP*-invariant scalar potential, namely, only the real parts of the two neutral scalars can mix with each other but not with the imaginary parts,

$$H\equiv c_\alpha\text{Re}[\Phi_1^0]+s_\alpha\text{Re}[\Phi_2^0],\qquad h\equiv -s_\alpha\text{Re}[\Phi_1^0]+c_\alpha\text{Re}[\Phi_2^0],$$
$$A\equiv -s_\beta\text{Im}[\phi_1^0]+c_\beta\text{Im}[\phi_2^0],\tag{4.1}$$

where $s_\alpha\equiv\sin\alpha$, $c_\alpha\equiv\cos\alpha$, $\tan\beta\equiv v_2/v_1$, and Re and Im denote the real and imaginary parts, respectively. Note that α is the mixing angle from the neutral scalar mass matrix diagonalization. The neutral particle masses are ordered as $m_H,m_A>m_h\approx 125$ GeV, so that h is the SM-like Higgs boson.

As in Ref. [14], we consider a very specific setup of the type III THDM, in which the tree-level flavor-changing neutral current couplings are present only in the lepton sector. The Yukawa interactions are given by

$$\mathcal{L}_Y=-\bar{L}Y_1\ell_R\Phi_1-\bar{L}Y_2\ell_R\Phi_2+\text{H.c.}\tag{4.2}$$

In this way, both Higgs doublets can contribute its neutral components to couple with the τ lepton [29],

$$-\frac{m_\tau}{v}\bar{\tau}_L\tau_R\left[\left(s_{\beta-\alpha}+\frac{N_{\tau\tau}}{m_\tau}c_{\beta-\alpha}\right)h+\left(c_{\beta-\alpha}-\frac{N_{\tau\tau}}{m_\tau}s_{\beta-\alpha}\right)H+iAN_{\tau\tau}\right]+\text{H.c.}\tag{4.3}$$

Here $c_{\beta-\alpha}\equiv\cos(\beta-\alpha)$, $s_{\beta-\alpha}\equiv\sin(\beta-\alpha)$, and $N_{\tau\tau}$ is a complex parameter related to the matrix elements of $Y_{1,2}$ [14], which is defined as

$$N_{\tau\tau}\equiv\frac{1}{m_\tau}N_{32}|M_{32}|.\tag{4.4}$$

In the weak basis, the mass matrix M_{ij} and the matrix N_{ij} with $i, j = 1, 2, 3$ are given by

$$M \equiv \frac{(Y_1 v_1 + Y_2 v_2)}{\sqrt{2}} \quad \text{and} \quad N \equiv -\frac{(Y_1 v_2 - Y_2 v_1)}{\sqrt{2}}. \tag{4.5}$$

Following the parametrization of Eq. (2.1), the τ Yukawa coupling becomes

$$\kappa_\tau(\cos\Delta + i \sin\Delta) = s_{\beta-\alpha} + \frac{N_{\tau\tau}}{m_\tau} c_{\beta-\alpha}. \tag{4.6}$$

Notice that CP violation arises due to the imaginary part of $N_{\tau\tau}$. For simplicity, we choose the Yukawa texture for $i, j = 2, 3$ as

$$Y_{1,2} \sim \begin{pmatrix} 0 & 0 \\ \times & \times \end{pmatrix}, \quad \text{and} \quad Y_{1,33} = Y_{2,33}. \tag{4.7}$$

Writing $Y_{1,32} = r_{32} Y_{2,32}$, we obtain that the imaginary part of a Jarskog-like invariant can be expressed as

$$\mathrm{Im}[J_A] = -\mathrm{Im}[r_{32}]|Y_{2,32}|^2 = \frac{2m_\tau^2}{v^2 c_{\beta-\alpha}} \kappa_\tau \sin\Delta, \tag{4.8}$$

which controls the size of the BAU in early Universe through lepton flavored baryogenesis [14]. Rewriting Eq. (4.8) gives

$$\sin\Delta = \frac{v^2 c_{\beta-\alpha}}{2m_\tau^2 \kappa_\tau} \mathrm{Im}[J_A]. \tag{4.9}$$

Thus, one may connect the τ Yukawa CP phase Δ, which can be measured at future lepton colliders, with CPV source for baryogenesis during the era of EWSB in the early Universe.

B. Sensitivity to the baryogenesis scenario

To make this connection concrete, we plot in Fig. 5 the 95% C.L. constraints on $\kappa_\tau \cos\Delta$ and $\kappa_\tau \sin\Delta$ from present and future collider probes and from lepton flavored EWBG. For generality, we also set $\kappa_\tau^{\text{test}}$ to be free to obtain a full picture on a two-dimensional plot. The CP sensitivity is then depicted as the contours around the true value $\Delta^{\text{true}} = 0°$ and $\kappa_\tau^{\text{true}} = 1$ in the left panel, with the green, blue (dashed), and red (dot dashed) contours indicating the 95% C.L. sensitivities. The green dotted lines from the origin $\kappa_\tau = 0$ are added to show that the contour size corresponds to roughly 7° at 95% C.L. Consistent with the previous observation, the CEPC and FCC-ee have comparable precision, while that of the ILC is slightly weaker due to different luminosities. For all three cases, the pink region allowing for successful explanation of BAU is outside the 95% C.L. contour. In other words, the lepton flavored BAU mechanism as given in Ref. [14] could be excluded at better than 95% C.L. For comparison, we also show the projected τ Yukawa CP measurement at the high luminosity (HL)-LHC [38] with the integrated luminosity of 3 ab^{-1} as the black contour, which will be further elaborated below. It is clear that even with the HL-LHC, the THDM BAU

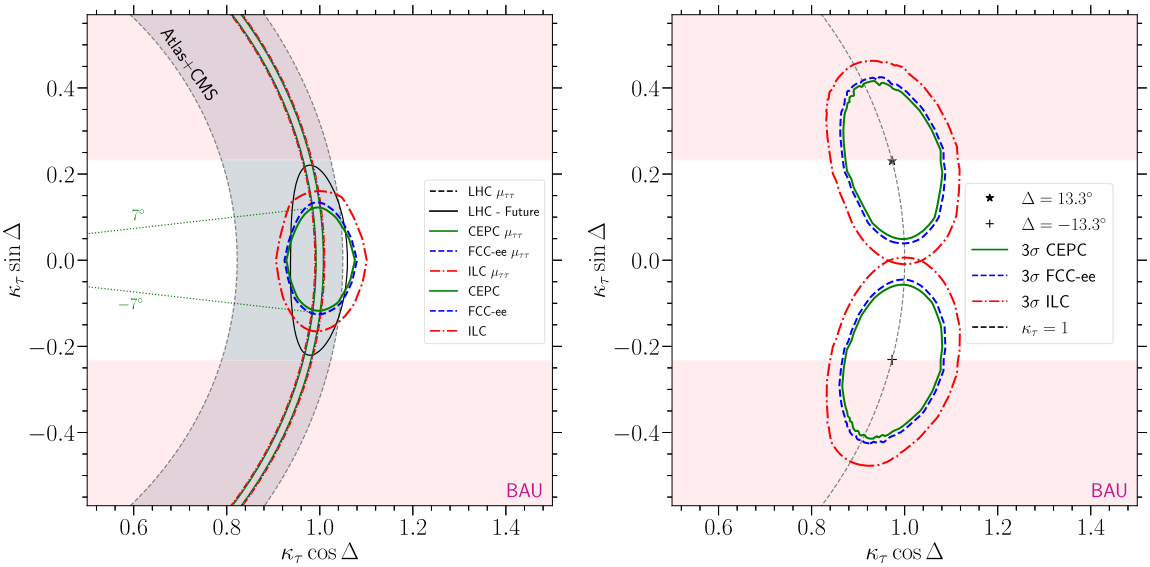

FIG. 5. Left: the 95% C.L. constraints on the τ Yukawa coupling at the CEPC (green), FCC-ee (blue), and ILC (red) assuming the true value $\Delta^{\text{true}} = 0°$ and $\kappa_\tau^{\text{true}} = 1$. The gray band gives 95% C.L. constraints from the current LHC signal strength measurements [5,6], while the black contour denotes the expected 95% C.L. constraint from the combined measurements of $\mu_{\tau\tau}$[60,61] and Δ[38] at the HL-LHC. Right: the 3σ contours for each collider assuming central values $\Delta^{\text{true}} = \pm 13.3°$ and $\kappa_\tau^{\text{true}} = 1$ corresponding to the minimum $|\kappa_\tau \sin\Delta|$ compatible with the BAU.

mechanism can only be tested with barely 95% C.L. The *CP* measurements at future lepton colliders can significantly improve the situation.

We also include the constraints from the measurement of the $h \to \tau\tau$ decay signal strength $\mu_{\tau\tau}$, which is proportional to κ_τ^2. The current data at the LHC indicate $\mu_{\tau\tau} = 1.09^{+0.35}_{-0.30}$ at ATLAS [5] and $\mu_{\tau\tau} = 0.85^{+0.12}_{-0.11}$ at CMS [6], which are depicted as the gray region. In other words, the current measurement at LHC is still quite crude with at least 10% uncertainty. At the HL-LHC, the 1σ uncertainty of $\mu_{\tau\tau}$ can be further improved to 5% [60,61], which is further combined with the *CP* measurement [38] that is shown as the black contour. The future lepton colliders can significantly improve the sensitivities to 0.8% at the CEPC [62], 0.9% at the FCC-ee [8], and 1.09% at the ILC [62], which are shown as the rings in the left panel of Fig. 5. Note that these rings with inclusive τ decays are much narrower than the width of the contours or, equivalently, the marginalized sensitivity on κ_τ after integrating out the *CP* phase Δ from the original two-dimensional distributions. The discrepancy comes from the fact that the $\tau \to \pi\nu_\tau$ and $\tau \to \rho\nu_\tau$ channels contribute only a very small fraction ($\sim$13%) of the inclusive decay events. The strength measurement can provide very important complementary info and reduce the parameter space to be explored.

Instead of assuming the SM values $\kappa_\tau^{\text{true}} = 1$ and $\Delta^{\text{true}} = 0°$, it is interesting to ask the whether the lepton flavored EWBG scenario can explain the BAU and at the same time produce a signal that is distinguishable from the SM. To address this question, we show in the right panel of Fig. 5 the similar contours around $\Delta^{\text{true}} = \pm 13.3°$ and $\kappa_\tau^{\text{true}} = 1$ that is at the boundary of the BAU region. Under this assumption, the CEPC and FCC could establish the presence of CPV in the τ Yukawa interaction with 3σ significance, while for the ILC the significance would be somewhat weaker.

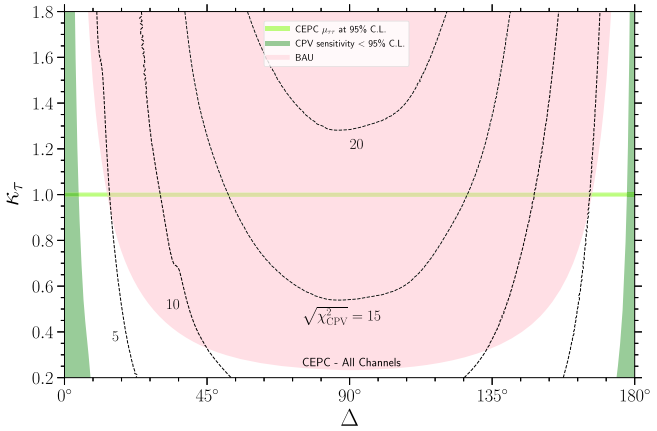

FIG. 6. The *CP* discovery capability of the CEPC as a function of the Δ and κ_τ true values. The black dashed lines represent several typical values of the significance, $\sqrt{\chi^2_{\text{CPV}}} = 5, 10, 15, 20$. The green region represents the space parameter where the sensitivity is below 95% C.L. The pink region represents the parameter space that can explain the BAU in the lepton flavored EWBG scenario [14].

It is also interesting to investigate the behavior of the *CP*-violation sensitivity when one varies the assumed true values of κ_τ. This can be observed from Fig. 6, where we show the sensitivity as a function of the *CP* phase Δ and the coupling strength κ_τ. The dashed gray lines give several typical sensitivities, $\sqrt{\chi^2_{\text{CPV}}} = 5, 10, 15, 20$. Note that the dashed gray lines expand with larger τ Yukawa coupling due to event number enhancement. This is especially significant for small κ_τ, while for large values of κ_τ the *CP* sensitivity does not change substantially. The BAU-compatible region has a lower limit at $\kappa_\tau \approx 0.25$ due to the lower limit on $\kappa_\tau \sin\Delta$ according to Fig. 5 and most of the BAU-compatible region falls inside the $\sqrt{\chi^2_{\text{CPV}}} = 5$ curve, corresponding to 5σ discovery.

V. CONCLUSIONS

Explaining the origin of the baryon asymmetry of the Universe is a key open problem at the interface of particle and nuclear physics with cosmology. An essential ingredient in the explanation is the presence of BSM *CP* violation. In the electroweak baryogenesis scenario, the relevant CPV interactions would have generated the BAU during the era of EWSB. The corresponding mass scale makes these interactions, in principle, experimentally accessible. While null results for permanent EDM searches place strong constraints on new flavor-diagonal, electroweak scale CPV interactions, flavor-changing CPV effects are significantly less restricted. Lepton flavored EWBG draws on this possibility, with interesting implications for CPV in the tau-lepton Yukawa sector.

In this work, we have shown how measurements of CPV observable in Higgs boson ditau decays at prospective future lepton colliders could test this possibility, with significant discovery potential if it is realized in nature. After making a detailed comparison of the four differential distributions of the neutrino azimuth angle $\delta\phi_\nu$, polarimeter $\delta\phi_r$, acoplanarity ϕ^*, and the Θ variable for the first time, as well as various detector responses, we explore the prospects of *CP* measurement in the τ Yukawa coupling at future lepton colliders. With $(5.6, 5, 2)$ ab^{-1} luminosity, the 1σ uncertainty can reach 2.9°, 3.2°, and 3.8° at the CEPC, FCC-ee, and ILC, respectively. This allows the possibility of distinguishing the attainable EWBG from the *CP*-conserving case with 3σ sensitivity. The future lepton colliders are not just precision machines for detailing our understanding of the Higgs boson, but can also make $\mathcal{O}(1)$ measurement of the possible new physics beyond the SM.

ACKNOWLEDGMENTS

S. F. G. is sponsored by the Double First Class start-up fund (WF220442604) provided by Tsung-Dao Lee Institute

and Shanghai Jiao Tong University, the Shanghai Pujiang Program (20PJ1407800), and National Natural Science Foundation of China (No. 12090064). S. F. G. is also grateful to Kai Ma for sharing his Ph.D. thesis with derivations on the differential distribution of the $\tau \to \pi\nu_\tau$ decay as well as Manqi Ruan, Xin Chen, and Dan Yu for useful discussions. G. L. would like to thank Shou-hua Zhu for helpful discussions. M. J. R. M. was supported in part under National Natural Science Foundation of China Grant No. 19Z103010239. G. L. and M. J. R. M. were supported in part under U.S. Department of Energy Award No. DE-SC0011095. This work is also supported in part by Chinese Academy of Sciences Center for Excellence in Particle Physics (CCEPP).

[1] G. Aad *et al.* (ATLAS Collaboration), Observation of a new particle in the search for the Standard Model Higgs boson with the ATLAS detector at the LHC, Phys. Lett. B **716**, 1 (2012).
[2] S. Chatrchyan *et al.* (CMS Collaboration), Observation of a new boson at a mass of 125 GeV with the CMS experiment at the LHC, Phys. Lett. B **716**, 30 (2012).
[3] S. Chatrchyan *et al.* (CMS Collaboration), Evidence for the 125 GeV Higgs boson decaying to a pair of τ leptons, J. High Energy Phys. 05 (**2014**) 104.
[4] G. Aad *et al.* (ATLAS Collaboration), Evidence for the Higgs-boson Yukawa coupling to tau leptons with the ATLAS detector, J. High Energy Phys. 04 (2015) 117.
[5] M. Aaboud *et al.* (ATLAS Collaboration), Cross-section measurements of the Higgs boson decaying into a pair of τ-leptons in proton-proton collisions at $\sqrt{s} = 13$ TeV with the ATLAS detector, Phys. Rev. D **99**, 072001 (2019).
[6] CMS Collaboration, Measurement of Higgs boson production in the decay channel with a pair of τ leptons, Report No. CMS-PAS-HIG-19-010.
[7] J. B. Guimarães da Costa *et al.* (CEPC Study Group), CEPC conceptual design report: Vol. 2—Physics and detector, arXiv:1811.10545.
[8] A. Abada *et al.* (FCC Collaboration), FCC-ee: The lepton collider: Future circular collider conceptual design report, Volume 2, Eur. Phys. J. Special Topics **228**, 261 (2019).
[9] H. Baer, T. Barklow, K. Fujii, Y. Gao, A. Hoang, S. Kanemura, J. List, H. E. Logan, A. Nomerotski, M. Perelstein *et al.*, The international linear collider technical design report—Vol. 2: Physics, arXiv:1306.6352.
[10] A. D. Sakharov, Violation of *CP* invariance, C asymmetry, and baryon asymmetry of the universe, Sov. Phys. Usp. **34**, 392 (1991).
[11] D. E. Morrissey and M. J. Ramsey-Musolf, Electroweak baryogenesis, New J. Phys. **14**, 125003 (2012).
[12] J. Engel, M. J. Ramsey-Musolf, and U. van Kolck, Electric dipole moments of nucleons, nuclei, and atoms: The standard model and beyond, Prog. Part. Nucl. Phys. **71**, 21 (2013).
[13] T. Chupp, P. Fierlinger, M. Ramsey-Musolf, and J. Singh, Electric dipole moments of atoms, molecules, nuclei, and particles, Rev. Mod. Phys. **91**, 015001 (2019).
[14] H. K. Guo, Y. Y. Li, T. Liu, M. Ramsey-Musolf, and J. Shu, Lepton-flavored electroweak baryogenesis, Phys. Rev. D **96**, 115034 (2017).
[15] C. W. Chiang, K. Fuyuto, and E. Senaha, Electroweak baryogenesis with lepton flavor violation, Phys. Lett. B **762**, 315 (2016).
[16] J. De Vries, M. Postma, and J. van de Vis, The role of leptons in electroweak baryogenesis, J. High Energy Phys. 04 (2019) 024.
[17] E. Fuchs, M. Losada, Y. Nir, and Y. Viernik, *CP* violation from τ, t and b dimension-6 Yukawa couplings—interplay of baryogenesis, EDM and Higgs physics, J. High Energy Phys. 05 (2020) 056.
[18] K. P. Xie, Lepton-mediated electroweak baryogenesis, gravitational waves and the 4τ final state at the collider, J. High Energy Phys. 02 (2021) 090.
[19] M. J. Ramsey-Musolf, The electroweak phase transition: A collider target, J. High Energy Phys. 09 (2020) 179.
[20] J. R. Dell'Aquila and C. A. Nelson, Usage of the $\bar{\tau}\tau$ or T anti-t decay mode to distinguish an intermediate mass Higgs boson from a technipion, Nucl. Phys. **B320**, 86 (1989).
[21] J. R. Dell'Aquila and C. A. Nelson, $\{CP\}$ determination for new spin zero mesons by the $\bar{\tau}\tau$ decay mode, Nucl. Phys. **B320**, 61 (1989).
[22] G. R. Bower, T. Pierzchala, Z. Was, and M. Worek, Measuring the Higgs boson's parity using tau → rho nu, Phys. Lett. B **543**, 227 (2002).
[23] M. Worek, Higgs *CP* from H/A0 → tau tau decay, Acta Phys. Pol. B **34**, 4549 (2003), https://arxiv.org/abs/hep-ph/0305082.
[24] K. Desch, Z. Was, and M. Worek, Measuring the Higgs boson parity at a linear collider using the tau impact parameter and tau → rho nu decay, Eur. Phys. J. C **29**, 491 (2003).
[25] K. Desch, A. Imhof, Z. Was, and M. Worek, Probing the *CP* nature of the Higgs boson at linear colliders with tau spin correlations: The case of mixed scalar-pseudoscalar couplings, Phys. Lett. B **579**, 157 (2004).
[26] S. Berge and W. Bernreuther, Determining the *CP* parity of Higgs bosons at the LHC in the tau to 1-prong decay channels, Phys. Lett. B **671**, 470 (2009).
[27] S. Berge, W. Bernreuther, and J. Ziethe, Determining the *CP* Parity of Higgs Bosons at the LHC in Their Tau Decay Channels, Phys. Rev. Lett. **100**, 171605 (2008).
[28] S. Berge, W. Bernreuther, B. Niepelt, and H. Spiesberger, How to pin down the *CP* quantum numbers of a Higgs boson in its tau decays at the LHC, Phys. Rev. D **84**, 116003 (2011).

[29] S. Berge, W. Bernreuther, and S. Kirchner, Prospects of constraining the Higgs boson's *CP* nature in the tau decay channel at the LHC, Phys. Rev. D **92**, 096012 (2015).
[30] J. R. Ellis, J. S. Lee, and A. Pilaftsis, CERN LHC signatures of resonant *CP* violation in a minimal supersymmetric Higgs sector, Phys. Rev. D **70**, 075010 (2004).
[31] S. Berge, W. Bernreuther, and H. Spiesberger, Higgs *CP* properties using the τ decay modes at the ILC, Phys. Lett. B **727**, 488 (2013).
[32] B. Grzadkowski and J. F. Gunion, Using decay angle correlations to detect *CP* violation in the neutral Higgs sector, Phys. Lett. B **350**, 218 (1995).
[33] R. Harnik, A. Martin, T. Okui, R. Primulando, and F. Yu, Measuring *CP* violation in $h \to \tau^+\tau^-$ at colliders, Phys. Rev. D **88**, 076009 (2013).
[34] A. Askew, P. Jaiswal, T. Okui, H. B. Prosper, and N. Sato, Prospect for measuring the *CP* phase in the $h\tau\tau$ coupling at the LHC, Phys. Rev. D **91**, 075014 (2015).
[35] K. Hagiwara, K. Ma, and S. Mori, Probing *CP* Violation in $h \to \tau^-\tau^+$ at the LHC, Phys. Rev. Lett. **118**, 171802 (2017).
[36] A. Bhardwaj, P. Konar, P. Sharma, and A. K. Swain, Exploring *CP* phase in τ-lepton Yukawa coupling in Higgs decays at the LHC, J. Phys. G **46**, 105001 (2019).
[37] T. Han, S. Mukhopadhyay, B. Mukhopadhyaya, and Y. Wu, Measuring the *CP* property of Higgs coupling to tau leptons in the VBF channel at the LHC, J. High Energy Phys. 05 (2017) 128.
[38] X. Chen and Y. Wu, Probing the *CP*-violation effects in the $h\tau\tau$ coupling at the LHC, Phys. Lett. B **790**, 332 (2019).
[39] A. K. Swain, M_{T2} as a probe of *CP* phase in $h \to \tau\tau$ at the LHC, arXiv:2008.11127.
[40] J. de Blas, M. Cepeda, J. D'Hondt, R. K. Ellis, C. Grojean, B. Heinemann, F. Maltoni, A. Nisati, E. Petit and R. Rattazzi *et al.*, Higgs boson studies at future particle colliders, J. High Energy Phys. 01 (**2020**) 139.
[41] D. Jeans and G. W. Wilson, Measuring the *CP* state of tau lepton pairs from Higgs decay at the ILC, Phys. Rev. D **98**, 013007 (2018).
[42] X. Chen and Y. Wu, Search for *CP* violation effects in the $h \to \tau\tau$ decay with e^+e^- colliders, Eur. Phys. J. C **77**, 697 (2017).
[43] CMS Collaboration, Analysis of the *CP* structure of the Yukawa coupling between the Higgs boson and τ leptons in proton-proton collisions at $\sqrt{s} = 13$ TeV, Report No. CMS-PAS-HIG-20-006.
[44] J. H. Kuhn and F. Wagner, Semileptonic decays of the tau lepton, Nucl. Phys. **B236**, 16 (1984).
[45] P. A. Zyla *et al.* (Particle Data Group), Review of particle physics, Prog. Theor. Exp. Phys. **2020**, 083C01 (2020).
[46] M. Benedikt, A. Blondel, P. Janot, M. Mangano, and F. Zimmermann, Future circular colliders succeeding the LHC, Nat. Phys. **16**, 402 (2020).
[47] T. Behnke, J. E. Brau, P. N. Burrows, J. Fuster, M. Peskin, M. Stanitzki, Y. Sugimoto, S. Yamada, H. Yamamoto, H. Abramowicz *et al.*, The international linear collider technical design report—Vol. 4: Detectors, arXiv:1306.6329.
[48] F. An, Y. Bai, C. Chen, X. Chen, Z. Chen, J. G. da Costa, Z. Cui, Y. Fang, C. Fu, J. Gao *et al.*, Precision Higgs physics at the CEPC, Chin. Phys. C **43**, 043002 (2019).
[49] J. Alwall, M. Herquet, F. Maltoni, O. Mattelaer, and T. Stelzer, MadGraph 5: Going beyond, J. High Energy Phys. 06 (2011) 128.
[50] K. Hagiwara, T. Li, K. Mawatari, and J. Nakamura, TauDecay: A library to simulate polarized tau decays via FeynRules and MadGraph5, Eur. Phys. J. C **73**, 2489 (2013).
[51] J. de Favereau, C. Delaere, P. Demin, A. Giammanco, V. Lemaître, A. Mertens, and M. Selvaggi (DELPHES 3 Collaboration), DELPHES 3, A modular framework for fast simulation of a generic collider experiment, J. High Energy Phys. 02 (2014) 057.
[52] A. Rouge, *CP* violation in a light Higgs boson decay from tau-spin correlations at a linear collider, Phys. Lett. B **619**, 43 (2005).
[53] M. Selvaggi, https://github.com/delphes/delphes/blob/master/cards/delphes_card_CircularEE.tcl, 2020.
[54] T. Abe *et al.* (Linear Collider ILD Concept Group), The international large detector: Letter of intent, CERN Document Server, arXiv:1006.3396.
[55] C. Chen, X. Mo, M. Selvaggi, Q. Li, G. Li, M. Ruan, and X. Lou, Fast simulation of the CEPC detector with DELPHES, arXiv:1712.09517.
[56] J. H. Kuhn, Tau kinematics from impact parameters, Phys. Lett. B **313**, 458 (1993).
[57] D. Jeans, Tau lepton reconstruction at collider experiments using impact parameters, Nucl. Instrum. Methods Phys. Res., Sect. A **810**, 51 (2016).
[58] V. D. Barger, J. L. Hewett, and R. J. N. Phillips, New constraints on the charged Higgs sector in two Higgs doublet models, Phys. Rev. D **41**, 3421 (1990).
[59] G. C. Branco, P. M. Ferreira, L. Lavoura, M. N. Rebelo, M. Sher, and J. P. Silva, Theory and phenomenology of two-Higgs-doublet models, Phys. Rep. **516**, 1 (2012).
[60] CMS Collaboration, Projected performance of an upgraded CMS detector at the LHC and HL-LHC: Contribution to the snowmass process, arXiv:1307.7135.
[61] ATLAS Collaboration, Projections for measurements of Higgs boson signal strengths and coupling parameters with the ATLAS detector at a HL-LHC, Report No. ATL-PHYS-PUB-2014-016.
[62] D. Yu, M. Ruan, V. Boudry, H. Videau, J. C. Brient, Z. Wu, Q. Ouyang, Y. Xu, and X. Chen, The measurement of the $H \to \tau\tau$ signal strength in the future e^+e^- Higgs factories, Eur. Phys. J. C **80**, 7 (2020); D. Yu, M. Ruan, V. Boudry, H. Videau, and J. C. Brient, Higgs to $\tau\tau$ analysis in the future e^+e^- Higgs factories, arXiv:1903.12327.